A Single Pixel Touchless Laser Tracker Probe

*Joshua A. Gordon, David R. Novotny, Alexadra E. Curtin
Radio Frequency Technology Division, National Institute of Standards and Technology
Boulder, CO 80305
*josh.gordon@nist.gov, (303)-497-4312

Abstract— We have developed a laser tracker probe, the Pixel Probe, that does not require physically contacting the object one is measuring and which has 3D spatial resolution of about 25 µm (in x,y,z) in the current configuration. This touchless laser tracker probe uses three machine vision cameras to discretize a scene down to the spatial resolution of a pixel. A single pixel from each camera field of view is linked to a laser tracker through a calibration process. The three pixels define a point in space that is used as a virtual touch probe where one places these pixels on an object by means of viewing the camera images. This allows one to measure with a laser tracker the location of small features (tens of µm) on an object without needing physical contact. Given that the design of this system is easily scalable to higher resolution cameras and lenses, it is envision that this system could provide better than the current 25 µm resolution. The Pixel Probe excels at measuring objects that may prove difficult for existing laser tracker probes such as sharp edges and corners, amorphous, soft, and intangible objects. In addition one can register to the laser tracker features that appear in the images, and or geometries that are derived using machine vision edge and feature recognition algorithms. With the Pixel Probe it is also envision that other physical quantities based on optical imaging can be linked to a laser tracker such as thermal infrared data, spectral and polarimetric data. We present the concept, design, function, calibration, and operation of this system, as well as measurements.

I. INTRODUCTION

Laser trackers (LT) are effective for the spatial characterization of solid objects and have found many uses in industrial applications for spatial metrology tasks such as robot calibration, 3D part characterization, tolerancing, and reverse engineering. They have also been indispensible in advanced surveying applications where high degrees of accuracy and precision are required such as in aircraft assembly and telescope observatories[1] . LTs have also been useful in the construction and alignment of antenna ranges and antennas[2,3,4] . The type of object that can be spatially characterized with these systems is dependent on the type of LT probe used. Perhaps the most common probe is the spherical mirror reflector (SMR) made from three perpendicular mirror surfaces forming the corner of a cube. The SMR can be used on its own as a stencil that can be moved along a surface in a spatial measurement. As typical SMRs are limited to 1" and 0.5" diameter spherical form factor, more complicated probes such as touch probes and laser line scanners have been developed to provide increased versatility for manual scanning of objects.

In the context of precision antenna alignments, LTs are very useful. They allow one to obtain hi-fidelity spatial information routinely less than 100 µm which is sufficient for antenna alignments[5] necessary at frequencies in the millimeter-wave (mm-wave) range (100 GHz-300 GHz). Currently available LT probes are excellent performers for many applications when the object of interest is significantly larger than the probe, made of solid material, can be physically contacted without deformation, has well characterized albedo, and lacking in sharp edges, or corners[6]. However, when the object does not meet such requirements, current LT targets may not be adequate. This scenario presents itself regularly when dealing with mm-wave components which have dimensions of interest that are on the order of 1 mm, have sharp corners and edges, are constructed of polished metal, and too delicate to touch. The need for a new type of LT probe that could provide useful spatial metrology of these mm-wave components is the motivating circumstance for this work.

This new LT probe, called the Pixel Probe, is unlike other probes in that it is based on optical imaging. The Pixel Probe prototype presented here uses three cameras nominally arranged in a tetrahedral which are constructed from three 2592x1944 CMOS pixel arrays (a.k.a focal plane arrays FPA) and three 12.5 mm focal length low distortion machine vision lenses. From each camera a single pixel is linked to a laser tracker through a calibration process we describe below. These three pixels are then used to unambiguously define a single point in space, P* that is known in the native coordinate frame of the LT. Because P* is defined through the camera images, it is in actuality a virtual object that is conjugate to the physical pixels in each FPA. As such, there is nothing physically there at the location of P* . In use, P* is defined as a set of pixel coordinates from each camera and can be virtually placed on the object we wish to measure by using the camera images. This is similar to the action performed when using a touch probe, or coordinate measurement machine (CMM). However, in this case nothing needs to physically touch the object under measure. The use of FPAs allows for spatial resolution on the order of tens of µm and also makes the spatial resolution of this approach scalable by judicious choices of FPA pixel size and lens focal length. The Pixel Probe prototype we present here has approximately 25 µm spatial resolution.

The non-contact imaging nature of the Pixel Probe allows novel measurement modalities not obtainable with other LT probes and targets, such as measuring sharp corners, sharp edges, objects that are soft, optically transparent, objects of high and low reflectance as well as virtual objects (such as an image of a real object). In addition other optical information such as geometries determined from machine vision algorithms, thermal infrared data, spectral and polarization information that represents other physical quantities could also be simultaneously linked to the spatial measurement of the LT. This provides a new type of measurement framework and opens up the ability to perform direct multi-physics measurements with a LT. Such measurements could be used to compare multi-physics simulations with real data, much like is done when CAD models are compared to point cloud data generated using a LT or CMM. The Pixel Probe can also be used for robot Tool Center Point (TCP) calibration and teaching with spatial resolution and accuracy on the order of tens of μm . The imaging properties of the Pixel Probe allow for robot tool end effectors to be measured that may be difficult to otherwise characterize, such as water jets or laser welding spots, etc.

Below we demonstrate the capability of the Pixel Probe by presenting data for several objects: 1) A validation measurement using a glass plate camera target grid made of 250 μm diameter electron beam etched chrome dots. The plane of this plate is measured using the Pixel Probe and compared to a measurement of the plane of the glass plate using a 1.5" SMR. 2) The 1.5 mm diameter aperture of a gold plated circular antenna, 3) the 12.55 mm x 9.58 mm rectangular aperture of a gold plated pyramidal horn antenna, 4) The shrinkage ratio of transparent Heat Shrink ® 5) A manmade spider web fabricated from strands of clear epoxy. These objects are all quite challenging to measure with traditional LT probes. They are either too delicate to touch, too small, their optical properties make them difficult to measure, or they have a combination of such attributes.

II. Concept of Operation

A. *Point Projection to a Pixel*

With the proliferation of CCD and CMOS cameras, it is not hard to find FPAs with pixel sizes on the order of a few μm with several megapixel densities. Furthermore, optical lenses with modulation transfer functions (MTF) above a hundred line pairs per mm are also easy to obtain to match these high resolution FPAs. It is therefore rather easy to achieve imaging resolution on the order of tens of μm . However, although this spatial resolution is readily obtained in the image plane transverse to the optical axis (OA), the spatial resolution along the OA is instead dictated by the depth of focus (DOF) of the lens and not pixel resolution. The DOF is the distance over which an object can be shifted along the OA while still remaining in focus. In a ray optics picture this distance can be considered to be zero. However, due to the wave nature of light in a real optical system, the DOF is a non-zero value that depends on the ratio of the focal length to lens aperture, i.e., the f-number denoted as F/#. The DOF for a rotationally symmetric lens can be closely modeled with a Gaussian beam. Consider the expression for a Gaussian beam generated by a lens. The DOF for such a beam[7] is,

$$DOF = \frac{8\lambda}{\pi}\left(F/\#\right)^2 \quad . \qquad (1)$$

If we want to measure the displacement of an object along the OA then we would want a relatively small DOF, such that we could determined the plane of our object to within the error provided by the DOF. From (1) we see that for small DOF we need small F/#. However this typically comes at the expense of a needing to bring the object we are imaging close the lens and also a decrease in image field of view . For instance, a 50X, F/0.9 microscope objective has very good DOF resolution of $\approx 1\ \mu m$, but with an object-to-lens distance (working distance) of only $\approx 1\ cm$, the field of view is $\approx 50\ \mu m$. In practice, we wish to have a respectable working distance (>100 mm), such that the camera lens does not interfere with the object we are trying to measure. At the same time it would be nice to have a field of view much greater than that of the microscope.

In contrast to a microscope objective, a typical machine vision lens has a comparatively long DOF of several millimeters, yet does provide transverse resolution of tens of μm , with a respectable field of view of tens of mm and working distance of hundreds of mm. For the system we present here, the camera lens and FPA used allow for roughly a 25 μm pixel resolution across a total FOV of roughly 3 cm x 3 cm at a working distance of 100 mm.

Using only a single lens to locate an object in three dimensions would result in good spatial discrimination of position of the object transverse to the OA in the image plane. However, this lens would produce a comparatively ambiguous measure of object location along the lens OA. Therefore in order to obtain the same spatial discrimination along the OA that can be achieved in the image plane, we need a way to break the ambiguity that results from the relatively long DOF of the lens.

We employ the concept of point projection onto multiple images planes to address the DOF ambiguity of a single lens. To accomplish this a three-camera approach is used. Three cameras are nominally oriented in a tetrahedral such that the OA of one camera is projected along the image plane of the others. This way a movement of a point along the OA of one camera is seen as a translation in the other two and thus the DOF ambiguity is broken. As such, the FPA of the other two cameras now provides the needed spatial resolution, and spatial discrimination along the OA of the third camera. In this way we achieve spatial resolution comparable to the FPA in three directions: along the two dimensions of the image plane and along the OA. This is depicted in Figure 1. P_1 (solid red dot) shown in Figure 1 is positioned on the OA of Camera 1 but located by some amount inside the plane of best focus, denoted as the Object Plane 1, but within the DOF of Camera 1. Point P_1 is at the same time being projected along Object Plane 2 of Camera 2 thereby creating point P_2 (red open circle). The image of P_1 in Camera 1 is see as P_1' (solid blue dot) and in Camera 2 as P_2' (open blue circle).

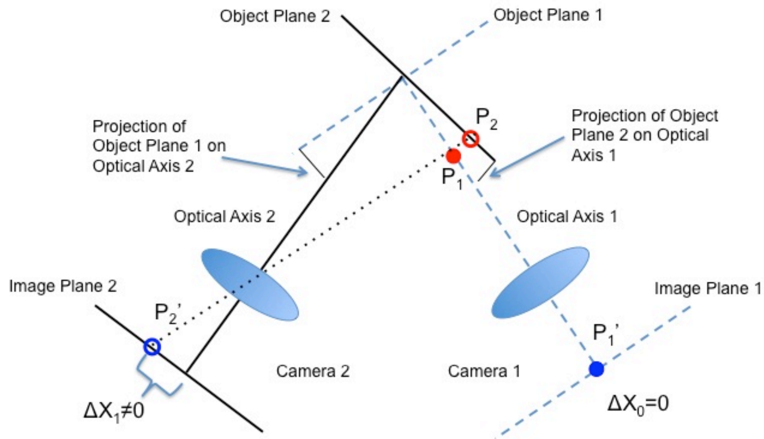

Figure 1. Point projection onto multiple image planes. P_1 (solid red dot) is positioned on the OA of Camera 1, but located by some amount inside the plane of best focus denoted as the Object Plane 1. Point P_1 (solid red dot) coincident with the OA of Camera 1 is projected along the object plane of Camera 2 creating point P_2 (red circle). The image of this point in Camera 1 is see as P_1' (blue dot) and in Camera 2 as P_2' (blue circle).

In Camera 1, P_1' remains in the center of Image Plane 1 with little detectable change, where as P_2' is seen to have shifted by a measurable number of pixels denoted by ΔX. The extent of the shift on Image Plane 2 depends on the physical shift of P_2 and by the image magnification dictated by the lens focal length of Camera 2 and the object image conjugate distances of P_2 and P_2'[7]. As such P_1 has three conjugate images, one on each camera. Although strictly speaking a point in space is infinitely small, given that one pixel represents the smallest discernable element in the image planes, P_1' and P_2' can at best be represented as a set of pixel coordinates. Therefore a given P_1 will have a unique set of two dimensional pixel coordinates (x_p, y_p) in each camera image. Thus using three cameras P_1 is specified with a set of 3 pixel coordinates, (x1p, y1p), (x2p,y2p), (x3p,y3p). If now we could link P_1 to a LT, such that these pixel coordinates define a point that is also known to the LT, P_1 becomes a LT probe with the spatial resolution of a single pixel. Next we discuss the process of defining the coordinates of P_1 in each of the three cameras while simultaneously linking P_1 to a LT coordinate system.

B. Linking a Pixel to a Laser Tracker

Using the principle of projection to the three image planes as was done for the single point P_1 , a sphere that is imaged by the three cameras will result in three circular images at each of the image planes. Furthermore, the centroid of these three circular images when projected back to the object plane are all coincident with the 3D center of the sphere. Therefore just as we were able to assign a unique set of three pixel coordinates to the single point, P_1 , we can assign a similar set of three pixel coordinates to the centroid of the sphere. As is commonly known, the geometrical center of an SMR is also coincident with the location that is measured by the LT to within a nominal alignment of 5 to 10 µm . Here in lies the trick. Because the cameras can identify the sphere center, by projection to the pixel arrays, as well as the LT can, we have a direct way to link the set of pixel coordinates of the sphere center to the LT. This is depicted in Figure 2.

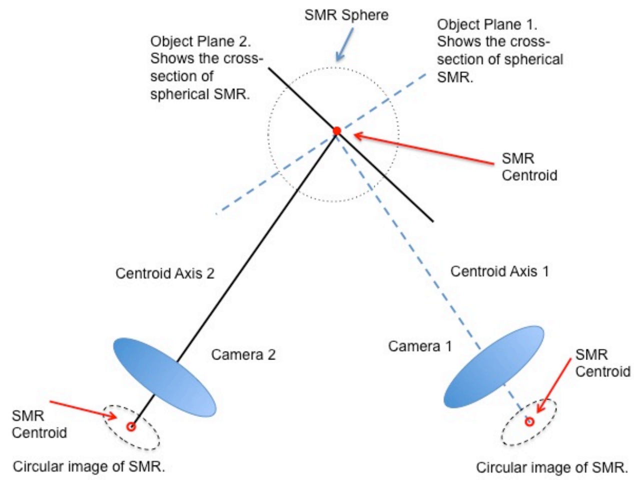

Figure 2. Projection of an SMR that is used to link the cameras to a laser tracker. The circular images in Camera 1 and 2 that are produced by the projection of the SMR are shown. The centroid of these SMR images coincides with the centroid of the spherical form of the SMR.

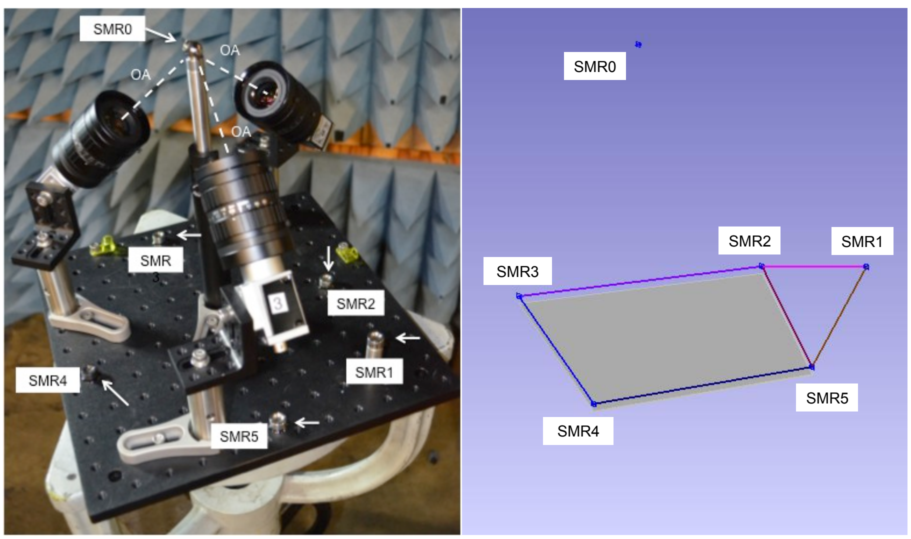

Figure 3. (Left) Pixel Probe prototype developed at NIST, Boulder. Three cameras are nominally arranged in a tetrahedral with a constellation of five SMRs fixed in relation to the cameras. The intersection of the optical axis (OA) for each camera to the location of SMR0 is shown. (Right) The points captured by the laser tracker representing the constellation of SMRs that is used to locate the Pixel Probe in the laser tracker coordinate frame.

The final Pixel Probe system prototype shown in Figure 3 is generated by establishing a fixed constellation of SMRs relative to the three cameras, one of which (called SMR0) is placed in the center of the FOV of the three cameras and plays the role of the sphere described previously. Five other SMRs are mounted to the base of cameras, SMR1 through SMR5. To link the laser tracker to a single pixel from each of the cameras, a bright field image of SMR0 is first captured by each camera (See Figure 4). A panel of light emitting diodes is used as to generate a Lambertian bright field background and a mat black shroud is placed around SMR0 and the cameras to stop unwanted reflections off the reflective SMR sphere. An edge detection algorithm is then used to determine the set of pixel coordinates that define the centroid of SMR0. Figure 4 shows the bright field image of SMR0. The red cross hairs locate the centroid, the green border is the region of interest (ROI) used in the edge detection process. Red dots on the perimeter of the SMR and inside the ROI are the location of the edge pixels determined from the edge detection algorithm. These three pixel coordinates are stored in memory and highlighted in the images of the three cameras. Although the entire sphere is not visible due to the SMR nest the validation measurement (see below) suggests the uncertainty from this does not significantly impact to the accuracy of this prototype. A future version of this prototype will address this.

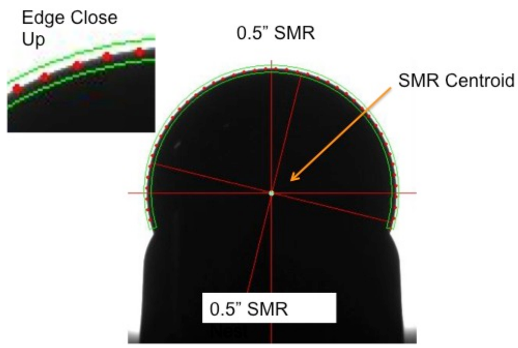

Figure 4. The bright field image of a 0.5 inch SMR as seen through the cameras of the Pixel Probe. This bright field image is the implementation of the SMR projection depicted in Figure 2. (Top Left) A close up of the SMR edge is shown. Green boundary is the ROI used for the edge detection process. Red dots show the location of the pixels at the SMR edge in the bright field. (Center) The centroid of the SMR determined from fitting a circle to the edge pixels is also shown.

While SMR0 remains in the same position relative to the cameras and the rest of the constellation (SMR1 though SMR5) the LT measures the entire constellation of SMRs. At this moment SMR0 can be *removed* from the constellation. This is because the centroid of SMR0 has been stored in memory as pixel coordinates, and these coordinates uniquely define the point in space of the centroid of SMR0 relative to the rest of the constellation. As such, when a point on an object appears to lie at the same location as the stored centroid pixels *in all three cameras simultaneously*, then that object occupies *the same location as centroid of SMR0 did*. In the current incarnation of the Pixel Probe, the stored pixels are highlighted in each of the three images. The user then moves the cameras such that these highlighted pixels appear at the same location on the object one is trying to measure. That is, the user is in essence virtually placing the centroid of SMR0 at a known location on the object of measure. At this moment the laser tracker then captures the rest of the SMRs in the constellation. Since the constellation has a fixed relationship to the centroid of SMR0 the location on the object under measure is also know by the LT. In this way we no longer need a physical LT target to touch the object we are trying to measure. In essence we have created a virtual LT probe that is the size of a single pixel, or about 25 µm in the prototype presented here. In the rest of this paper we will refer to the point in space corresponding to the centroid of SMR0 just as SMR0. At this time it is worth mentioning that although for this prototype, a constellation of SMRs is used in conjunction with SMR0, it would be equally effective to establish a coordinate frame using a six-degree-of freedom LT target that had a fixed relationship to SMR0. This would have advantages such as easier tracking ability and quicker measurement time, as the processing of the SMR constellation relationship to SMR0 would not be needed. Next we describe the validation and measurements made with the Pixel Probe.

III. MEASURMENTS

A. Validation Measurment

A validation measurement was performed to compare the performance of the Pixel Probe to a standard 1" SMR. A glass 2"x2" plate camera test target grid made of 250-µm -diameter electron-beam-etched chrome dots spaced by 500 µm was used. Since the grid dots are only a few hundred nanometers out of the plane of the glass, the dots are not distinguishable from the plane of the glass using a LT. This allows for a comparison measurement of the plane of the test target to be made between the SMR and Pixel Probe. As the Pixel Probe excels at measuring small features and the SMR excels at measuring surfaces, this test target combines both such aspects into a single geometry. The dots provide repeatable fiducials for the Pixel Probe to measure in the plane of the grid. While the optically flat glass substrate provides a repeatable surface for the SMR to measure. A spatial scan was performed as the SMR was moved along the surface of the glass grid. The Pixel Probe was used to measure several dots in the grid. Planes were then fitted to the individual data sets and the displacement and angular deviation of the normal were compared. Two SMR planes were measured and compared to the plane determined by the Pix Probe. This is shown in Figure 5. The rms fit statistics for the Pixel Probe plane was, 0.0021 mm, and the two SMR measured planes 0.0038 mm and 0.0039 mm respectively. This yielded a mean plane offset between the Pixel Probe measured plane and SMR measured planes of 19.5 µm , with an angular deviation of 0.11° . Both of these values are within the uncertainty of the LT.

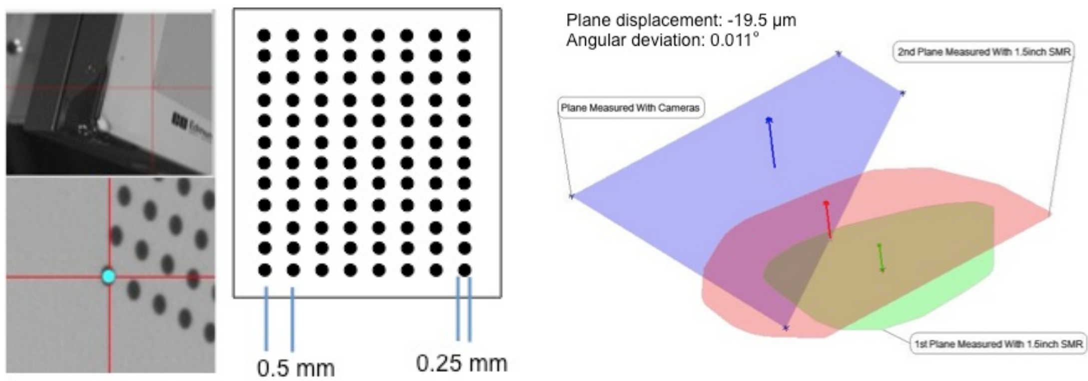

Figure 5. (Left) Grid test target. Square grid of 0.25 mm diameter chrome dots spaced by 0.5 mm. Full field and zoomed in images of the test target as seen in the Pixel Probe images are also shown. In the lower left SMR0 is located at the blue dot at the intersection of the red cross hairs. (Right) A visual comparison of planes determined from fits to data from the Pixel Probe (blue plane) and the 1" SMR (Red and Green Planes) measurements. A mean plane displacement of 19.5 µm and mean angular deviation of 0.11° was determined.

B. Measuring Millimeter-Wave Antenna Apertures

Next we show measurements of two mm-wave antenna apertures. A circular probe antenna and a pyramidal horn antenna with a rectangular opening are measured. These antennas are shown in Figure 6. The manufacture specified dimensions for the circular aperture is 1.5 mm diameter and 12.55 mm x 9.58 mm for the rectangular aperture. Both of these antennas are gold plated, are defined by sharp edges and quite delicate. For the purposes of antenna metrology[8] it is important to define a coordinate frame for these antennas based on the plane, center, and orientation of the aperture using a LT. These antennas are typically fixed to a mechanical positioner that is tracked with a LT. Therefore it is also important to know the antenna frame relative to the other LT targets that are used to track the positioner. Recent advances in antenna scanning systems use these antennas as the end effector tool of a robot arm[8]. Having a way to teach the robot the location of the antenna frame (i.e. tool tip frame) was one of the motivating factors in developing the Pixel Probe. As these antennas are much smaller than an SMR, and too delicate to touch, and require alignment accuracy of better than 50 µm , currently available methods for tool tip calibration were not suitable. The Pixel Probe not only allows for tool tip calibration through the robot controller routines, but allows for directly measuring the offset between the antenna aperture frame (i.e. tool tip) and a six-degree-of-freedom target or set of SMRs fixed on the robot.

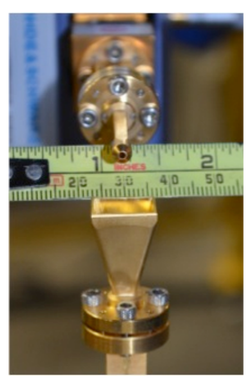

Figure 6. Circular probe antenna with nominal aperture radius of 1.5 mm and pyramidal horn antenna with rectangular aperture of nominal dimensions 12.55 mm x 9.58 mm.

The Pixel Probe was used to trace out the edges of these antenna apertures. Geometries were then fitted to determine the center, plane, and orientation of each antenna aperture. Figure 7 and 8 show the Pixel Probe measurements and the fitted geometry for the circular probe and pyramidal horn respectively. The circular aperture of the probe antenna was measured at 15 locations around the perimeter. These data were then fitted to a circle to determine the plane and diameter of the aperture. The circle fitting resulted in a diameter of 1.486 mm with an rms fit error of 22 µm . This is consistent with the manufacturer specifications of a 1.5 mm diameter aperture. The center and plane of this circle were used to define the coordinate frame of the probe antenna. The orientation of this frame in the plane of the circle was left arbitrary until an electrical alignment referenced to the plane of electric-field polarization to the test antenna was later performed.

The four corners of the pyramidal horn aperture were measured to determine the aperture dimensions. A rectangle was then fitted to these corners. A coordinate frame for the aperture was then defined in the plane of the rectangle and clocked to the short end of the rectangle. Figure 8 shows the measurement of the four corners and the resulting coordinate frame. The dimensions of the rectangular aperture determined from these measurements was 12.65 mm x 9.68 mm x 12.63 mm x 9.68 mm with a fit error of ≈ 20 μm which is in good agreement with the manufacturer specifications of 12.55 mm x 9.58 mm.

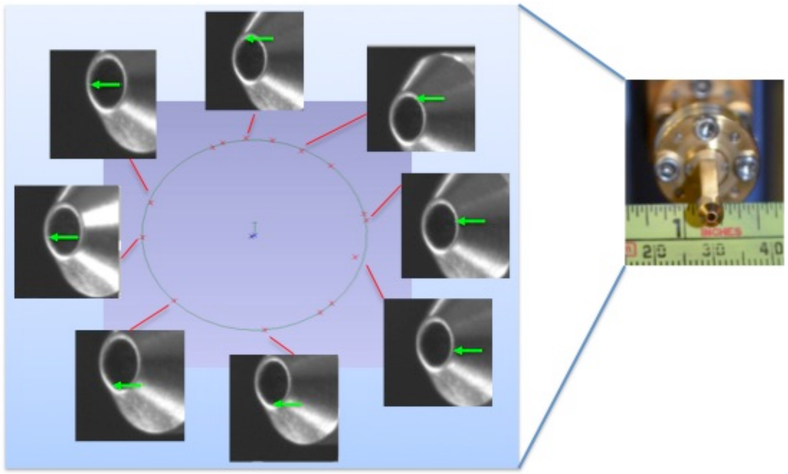

Figure 7. (Left) In the center of figure shows the circle that was fitted to measurements made with the Pixel Probe around the perimeter of the antenna aperture. Red data points lie along this fitted circle. At each measurement location an inset photo of the aperture as seen with the Pixel Probe is shown. In each inset photo a green arrow points to locations on the aperture where the Pixel Probe obtained measurements. (Right) Photo of the circular probe antenna. A ruler is also shown for scale. The diameter of this antenna aperture determined from the Pixel Probe measurements was 1.486 mm with an rms fit error of 22 μm .

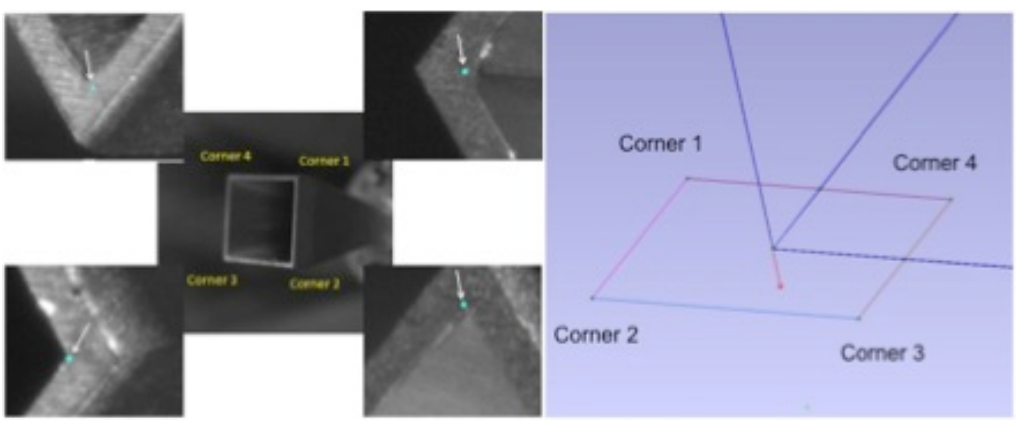

Figure 8. (Left) The corners of the pyramidal horn antenna measured with the Pixel Probe. White arrows point to blue dots which define the locations at which the corners 1,2,3,4 were measured. (Right) Coordinate frame generated using these corners. The dimensions of aperture were determined to be 12.65 mm x 9.68 mm x 12.63 mm x 9.68 mm with a fit error of ≈ 20 μm.

C.   Measuring Transparent and Soft Objects with a Laser Tracker

The imaging and non-contact measuring capability of the Pixel Probe allows for soft material to be measured with a LT without deforming the object. Furthermore, the imagining capability allows for objects constructed of weak albedo (low optically reflecting) material to be measured. We demonstrate this by measuring two objects with these attributes. First, measurements to determine the shrink ratio of clear Heat Shrink® (mention of this product is not an endorsement but is used to clarify what was done in this work) before and after shrinkage were made. Second, the geometry of a man made spider web constructed from strands of clear epoxy was measured. This is an extreme case of an object with these attributes and that is not easily measured with a LT, but that can be routinely measured with the Pixel Probe.

The shrink ratio of the material we used was 2:1 such that it should shrink twice as its original size. However Heat Shrink® is anisotropic in its shrinking behavior, such that it is designed to shrink only in one direction according to the specified shrink ratio, and not shrink in the orthogonal direction. A tube of Heat Shrink® was cut lengthwise to form a rectangle and fixed to a foam board with thumb tacks. Prior to shrinking a permanent marker was used to mark the Heat Shrink® along the direction of least shrinkage and most shrinkage. Figure 9 (Left) shows the Heat Shrink® fixed to the foam board with thumbtacks prior to shrinking. The thumbtacks were numbered 1 through 4 so as to avoid accidental confusion with the orientation Heat Shrink ® during measurement. Figure 9 (Right) shows the measured marks with the Pixel Probe prior to shrinking. They are labeled Mark 1-2, 2-3, 3-4, 4-1 and Mid Mark for the thumbtacks they lie between. Because the Heat Shrink® was meant for use as wire sheathing the non-shrinking direction was taken as along the direction of the tube prior to cutting. Using the Pixel Probe the separation between marks 2-3 and the mid mark and, 3-4 and the mid mark was measured to be 18.74 mm and 21.77 mm respectively. After shrinking the separation of these marks measured to be 6.89 mm and 22.67 mm. This gave a shrink ratio in the two directions of 2.77 and 0.96. This shows anisotropic shrinkage a bit larger than a 2:1 ratio. As a heat gun was used to shrink the material, the temperature applied was not as controlled as may be required by the manufacturer. This may be the biggest reason for the discrepancy between in the measured shrink ratio to the specified one.

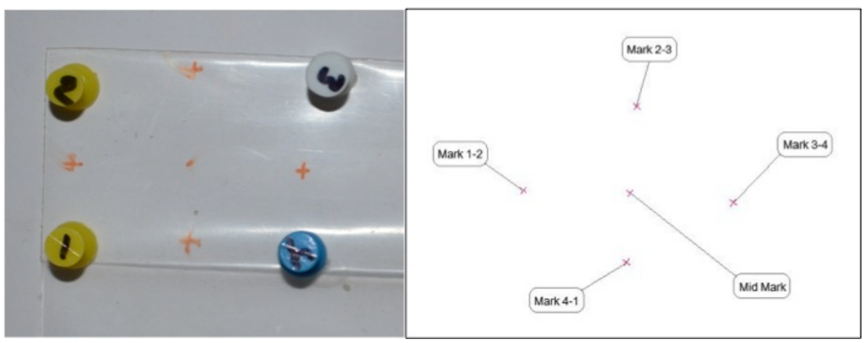

Figure 9. (Left) Clear Heat Shrink ® fixed to foam board with thumb tacks. Orange marks used to determine shrink ratio are shown. Numbered thumbtacks are also visible. (Right) Pixel Probe spatial data for the Heat Shrink ® .

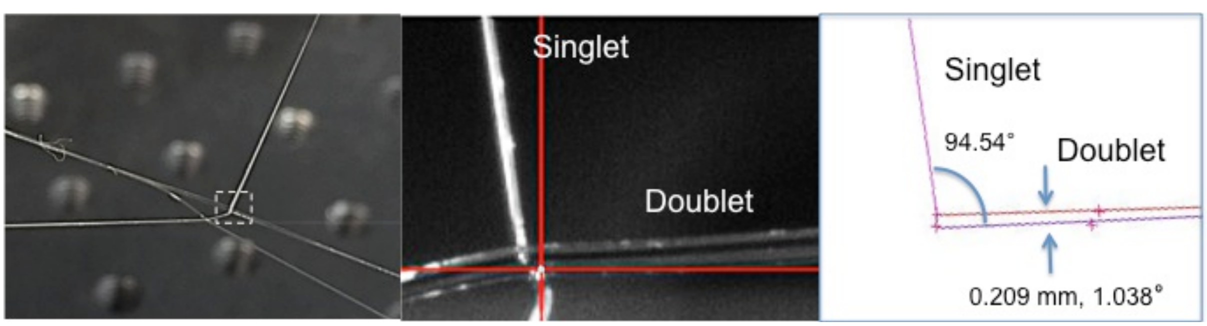

Figure 10. (Left) Photograph of the spider web made from stands of clear epoxy. ¼-20 holes on 1” centers in the optics bread board supporting the web are also visible in the background. Within the dotted box lies the junction of web strands that were measured with the Pixel Probe. (Middle) Close-up image through the pixel probe of the web strands. Red cross hairs mark the location of the SMR0 pixel. A singlet and doublet strand were identified to be measured. (Right) Spatial data plot for the geometry of the singlet and doublet strands. Angle between doublet members was determined to be 1.038° with a mean separation distance of 0.209 mm. The angle between the singlet and doublet was determined to be 94.54°.

The spider web was supported by metal posts screwed to a small optical bread board that had ¼-20 tapped holes on 1" centers. The web was measured at several locations along strands and at the points of strand intersection. The dotted box in Figure 10 (Left) shows the region of the web measured using the Pixel Probe. Figure 10 (Center) shows the close up view through the Pixel Probe. The intersection of the red crosshairs mark the location of the SMR0 pixel. A singlet and doublet set of strands were identified to be measured. From these data the geometry of the spider web was determined, and the separation of the members of the doublet was determined as well as the angle made between the singlet and doublet. The angle between individual doublet members was determined to be 1.038° with a mean separation distance of 0.209 mm. The mean angle between the singlet and doublet was determined to be 94.54°. This is shown in Figure 10 (Right).

D. Linking Machine Vision Derived Geometries To A Laser Tracker

Another aspect of the Pixel Probe is that geometries that are derived from machine vision algorithms can be directly linked to the LT. An example of this is given for the circular antenna probe aperture in Figure 11. In Figure 11 a ROI is defined in the images of the Pixel Probe around the circular aperture. An edge detection algorithm is then applied within the ROI to find the edge of the aperture. An ellipse fitting algorithm is then used to find the center of the aperture. Once the ellipse center is determined the SMR0 point in the Pixel Probe image is then placed at the same location as the ellipse centroid. At this moment the centroid of the ellipse is now linked to the LT. Figure 11 shows one image from the Pixel Probe depicting this process. The ROI is shown as the green boarder. The red boarder is made of highlighted pixels that were determined from the edge detection algorithm. These pixels define the edge of the aperture and are used to fit the ellipse. The red cross hairs are the major and minor axis of the ellipse. The yellow circle is the fitted ellipse centroid. The blue circle is the location of SMR0 from the Pixel Probe. When the blue circle and yellow circle overlap in the Pixel Probe images then the location of SMR0 and the centroid of the ellipse are in the same location in space. At this moment the ellipse centroid becomes linked to the LT. Furthermore, the error in the alignment between the yellow and blue circles can determined in real-time from calculating the pixel offset from the center of each circle. Although we have not deliberately calibrated how this pixel offset error translates into X,Y,Z errors in the LT frame, we envision a volumetric calibration could be preformed to provide X,Y,Z tacking of alignment errors and is the topic of future work. This would allow direct tracking of errors between the Pixel Probe SMR0 point and machine vision derived geometries. An application of this technique is for non-contact robot TCP calibration. This technique is used at the NIST Configurable Robotic Millimeter-Wave Antenna (CROMMA) Facility[8] to teach the robot arm the location of the center of the circular probe antenna aperture end effector. The robot arm is driven to five different poses, such that for all poses the TCP remains at the same point in space. This point in space is defined using the SMR0 point of the Pixel Probe. For each pose of the robot arm, the center of the circular probe aperture is determined using the edge detection and ellipse fitting algorithms just described. The robot is driven such that the center (yellow circle) of the fitted ellipse is aligned to the SMR0 point (blue circle) in the Pixel Probe just as is shown in Figure 11. Figure 12 shows the robot arm of the CROMMA in four of the five robot poses used to teach the robot controller the TCP location.

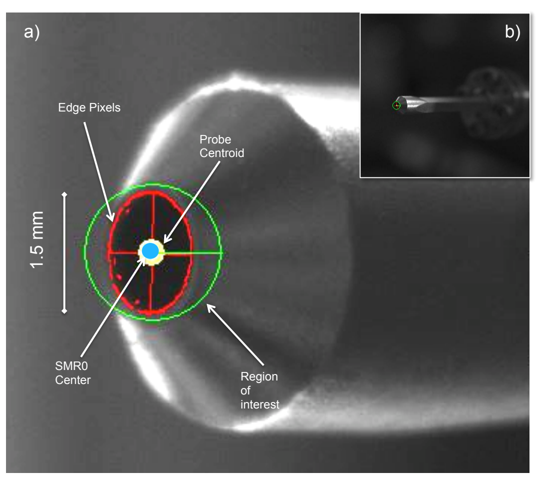

Figure 11. (a) Close up image of circular probe antenna (b) and full field view. Edge detected pixels (Red), circular probe centroid (Yellow), SMR0 center (Blue), and region of interest (Green) are shown.

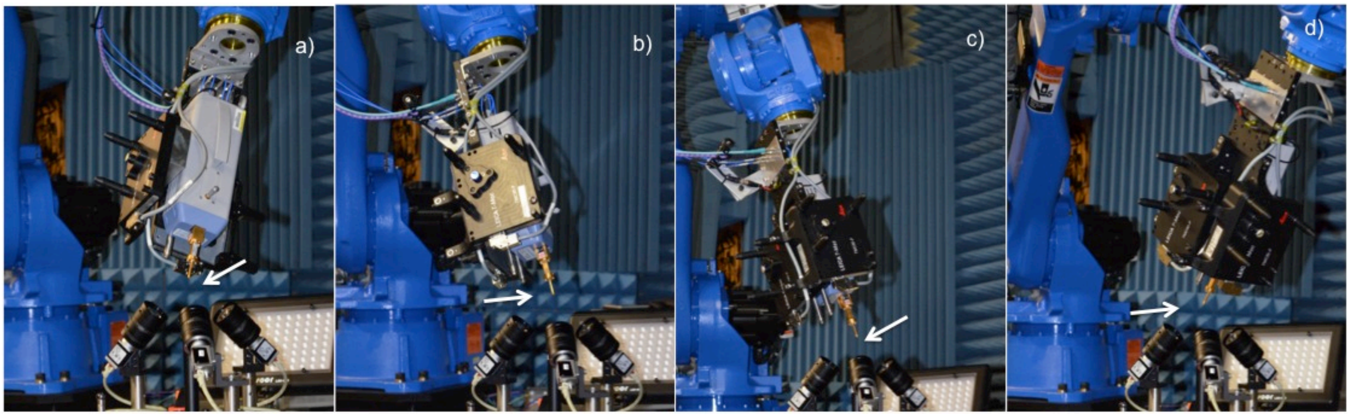

Figure 12. The robotic arm in the CROMMA facility. The Pixel Probe is mounted to a tripod while the robot arm is driven to the five poses (a)-(d) required of the TCP teach process. The circular probe antenna is the robot end effector. Only four poses are shown for brevity. White arrows point to the end of the antenna that is co-located with the SMR0 point of the Pixel Probe during the TCP calibration process.

IV. CONCLUSION

We have demonstrated a new laser tracker probe, the Pixel Probe, based on the projection of a point in space to an individual pixel in three separate image arrays. This point is inked to a laser tracker such that it forms a laser tracker probe with an effective size of a single pixel, about 25 µm . Given that the design of this system is easily scalable to higher resolution cameras and lenses, it is envision that this system could provide better than the current 25 µm resolution. We give a conceptual description of this new laser tracker probe, including how spatial projections are used to link the pixel to the laser tracker. We then present several types of spatial data obtained with the Pixel Probe of objects that would be difficult or extremely challenging to measure using existing laser tracker probes. These include measuring the sharp edge and corners small (1.5 mm) gold plated antennas, the shrink ratio of clear Heat Shrink® , and the linear and angular separation of strands in a manmade spider web constructed of clear epoxy. We also demonstrate how this probe can be used for robot tool center point calibration as well as registering geometries derived from machine vision algorithms to a laser tracker. Further applications that exploit the imaging nature of this probe are also discussed. These include directly registering laser tracker spatial data with other physical quantities that can be derived from spectral, polarization, and or infrared thermal imagining, and is a topic of our future work on this probe. This could provide a new type of measurement framework where physical quantities are directly measured in conjunction with highly accurate mechanical boundary conditions. This would allow the ability to perform direct multi-physics measurements with a laser tracker. Such measurements could be used to compare multi-physics simulations with real-world data much like is done when mechanical CAD models are compared to real-world surface measurements obtained from a laser tracker or CMM.

V. REFERENCES

[1] Rakich, A., "Alignment of LBT optics using a laser tracker", *Proc. SPIE* 7733, Ground-based and Airborne Telescopes III, 77335K, August (2010)

[2] Leon-Huerta, Andrea , et. al., " Alignment of a large outdoor antenna surface using a laser tracker ", Proc. SPIE 8788, Optical Measurement Systems for Industrial Inspection VIII, 878839 , May (2013)

[3] G., Hindman, A., Newell, et.al. , "Alignment Sensitivity and Correction Methods for Millimeter- Wave Spherical Near-Field Measurements", 2010 Proceedings of the Antenna Measurement Techniques Association, (2010).

[4] Wysock, Rousseau, et. al., "Using a Tracking Laser Interferometer to Characterize the Planarity of a Planar Near-Field Scanner", 2002 Proceedings of the Antenna Measurement Techniques Association, (2002).

[5] Francis, M.H, Wittmann, R. C., "Modern Antenna Hand Book", C. A. Balanis, Chp. 19, 929, (2008)

[6] Boehler, W. , Bordas Vicent, M. , Marbs, A. , "Investigating Laser Scanner Accuracy, CIPA (Scientific Committee for Documentation of Cultural Heritage) Symposium, Antalya Turkey, (2003)

[7] Greivenkamp , J. E., "Field Guide To Geometrical Optics", SPIE, Bellingham, WA , pp. 3, (2004)

[8] Gordon, J. Novotny, D., et. al., "The CROMMA Facility at NIST Boulder: A Unified Coordinated Metrology Space for Millimeter-Wave Antenna Characterization", Proceedings of the Antenna Measurement Techniques Association, (2014)